Excitation Gap in the Normal State of Underdoped $Bi_2Sr_2CaCu_2O_{8+\delta}$

A. G. Loeser, Z.-X. Shen, D. S. Dessau,* D. S. Marshall, C. H. Park, P. Fournier,† A. Kapitulnik

Angle-resolved photoemission experiments reveal evidence of an energy gap in the normal state excitation spectrum of the cuprate superconductor $Bi_2Sr_2CaCu_2O_{8+\delta}$. This gap exists only in underdoped samples and closes around the doping level at which the superconducting transition temperature T_c is a maximum. The momentum dependence and magnitude of the gap closely resemble those of the $d_{x^2-y^2}$ gap observed in the superconducting state. This observation is consistent with results from several other experimental techniques, which also indicate the presence of a gap in the normal state. Some possible theoretical explanations for this effect are reviewed.

The high-temperature superconductors (HTSs) have a temperature-dopant phase diagram with particularly rich physics, which has yet to be described by a single, consistent theory. In the undoped case, the copper oxide planes in HTS materials have an odd number of electrons per unit cell and are antiferromagnetic Mott-Hubbard insulators. The strong Coulomb interactions between the localized Cu 3*d* electrons suppress the charge mobility and make an insulator out of a crystal that band theory predicts should be a metal. On the other side, at high dopings in the copper oxide planes, the HTSs are metallic and display a band structure whose Fermi surface is consistent with local density approximation (LDA) band calculations (neglecting the contribution from the Bi-O pocket). These two cases are extremes at which the approximations that facilitate the respective theories are most accurate. However, the most intriguing physics, the superconductivity, exists (at low temperatures) at dopings between these two limits. Even the normal state physics of this regime is not well understood; although nominally metallic, it exhibits several physical properties different from those of conventional metals (*1*). With the idea of searching for qualitative signs of the crossover from one model to another, we investigated the doping dependence of the low-energy electronic structure in the normal state.

Recently, experimental evidence has been accumulating for the existence of another region in the HTS phase diagram, characterized by an excitation gap in the normal state. Several different measurements have indicated the presence of this gap in underdoped HTS samples (dopings below optimal, or that with the highest T_c). Analysis of the specific heat and thermoelectric power data of underdoped $YBa_2Cu_3O_{7-\delta}$ and Zn-doped $YBa_2Cu_4O_8$ shows a pseudogap in the normal state (*2*). In addition, an excitation gap is also deduced from the suppression of the in-plane scattering rate, measured by infrared reflectivity (*3*). Indirectly, this gap is inferred from transport properties; analyses of the Hall coefficient and uniform susceptibility of underdoped samples reveal a temperature scale T^* below which there appears to be a gap (*4*). This temperature scale increases very quickly as the samples become more underdoped, with T^* reaching as high as 600 K. In the spin channel, an excitation gap (spin gap) is observed in both nuclear magnetic resonance (NMR) and inelastic neutron scattering data (*5*, *6*). The interpretations of these experiments build a coherent, qualitative picture, although the details are not in precise agreement. For example, when the Cu NMR data are analyzed in terms of the maximum of $1/T_1T$ (where T_1 is the relaxation time), they reveal a gap that has a lower energy scale than that implied by T^* (*5*).

We report direct evidence for a gap in the single electron excitation spectrum obtained from angle-resolved photoemission spectroscopy (ARPES). Our data suggest that this excitation gap exists only in the underdoped samples and disappears close to the doping level at which T_c is maximized. This observation is connected to all of the experiments mentioned above, because the single electron excitation spectrum couples to both the spin and charge channels. Furthermore, the momentum-resolved nature of ARPES allows us to show that the excitation gap has a highly anisotropic momentum dependence. The magnitude and anisotropy of this gap are qualitatively similar to those of the superconducting gap observed below T_c in nearly optimally doped samples, which was interpreted as evidence for at least a significant component of $d_{x^2-y^2}$ pairing in the superconducting state (*7*). The similarity between these excitation gaps leads us to theoretical models that involve Cooper pair formation without long-range phase coherence at temperatures well above the superconducting regime. Our observations are consistent with these models, which in turn imply that the superconducting transition in underdoped crystals is fundamentally different from that predicted by conventional Bardeen-Cooper-Schrieffer (BCS) theory (*8*). In these models, the superconductivity occurs in the underdoped regime when the phases of the pairs become coherent, not when the pairs are first formed.

Experimental. In an ARPES experiment, electrons in a solid are excited above the vacuum level by incident monochromatic photons, and the energy and emission angle of the emitted electrons are measured. If the electronic states in the solid are two-dimensional (2D) in nature, then energy and momentum conservation laws imply a simple one-to-one mapping (at a given kinetic energy) between the electron's angle of emission and its momentum inside the solid. This is the case to a good approximation for many high-T_c superconductors, particularly for $Bi_2Sr_2CaCu_2O_{8+\delta}$ (Bi2212), which facilitated our detailed studies in momentum space. Within the commonly accepted sudden approximation (*9*), the resulting ARPES spectrum is the momentum-resolved (**k**-resolved) electron-removal excitation function added to a featureless background (*10*), and that is how we analyze our data. The ARPES data have an especially clear meaning in the further idealization of the quasi-particle picture. In this case, the presence of a feature at a given value of **k** corresponds to a filled quasiparticle band at that energy and momentum. The ARPES spectra from a set of different momenta can be used to determine the occupied part of the band's energy dispersion diagram. At momenta where the band is above the Fermi level (E_F), the occupation goes to zero, and the feature is not visible in the ARPES spectra. In the vicinity of this change from an occupied to

A. G. Loeser, Z.-X. Shen, and C. H. Park are in the Department of Applied Physics, Stanford Synchrotron Radiation Laboratory, and Solid State Laboratory, Stanford University, Stanford, CA 94305, USA. D. S. Dessau is with the Stanford Synchrotron Radiation Laboratory, Stanford University, Stanford, CA 94305, USA. D. S. Marshall is with the Solid State Laboratory, Stanford University, Stanford, CA 94305–4055, USA. P. Fournier and A. Kapitulnik are in the Department of Applied Physics, Stanford University, Stanford, CA 94305, USA.

*Present address: Department of Physics, University of Colorado, Boulder, CO 80309–0390, USA.
†Present address: Department of Physics, University of Maryland, College Park, MD 20742, USA.

unoccupied band, the **k** value at which the feature has lost 50% of its intensity is identified as a point on the Fermi surface. This idealization serves as a guide for our interpretation, although, as we explain below, the material in our experiment only approximates the quasi-particle behavior.

We report ARPES results (*11*) from bulk Bi2212, taken from crystals with a variety of oxygen contents (*12*, *13*). The optimal T_c of Bi2212 is 92 K, and samples with lower T_c are either underdoped or overdoped; which side of the curve a particular sample was on was known from the type of anneal used, reducing or oxidizing (*13*). As evidence of general sample quality and uniformity, the transition widths were between 1 and 2 K. All of the samples used in this study were superconductors, and for each, T_c was above 70 K.

To illustrate the doping dependence in the normal state, we first present data from three samples with different oxygen concentrations. The values of T_c for all samples were close to optimal but from two distinct areas in the phase diagram (Fig. 1). For our purposes, the superconducting transition curve is an approximate guide, because the maximum T_c obtainable with our crystals is slightly higher than the peak of the curve in the Fig. 1 (which could, for example, be a result of differences in cation stoichiometries). This simple method allows us to translate from T_c measurements to approximate Cu-O_2 plane dopings and locate specific photoemission

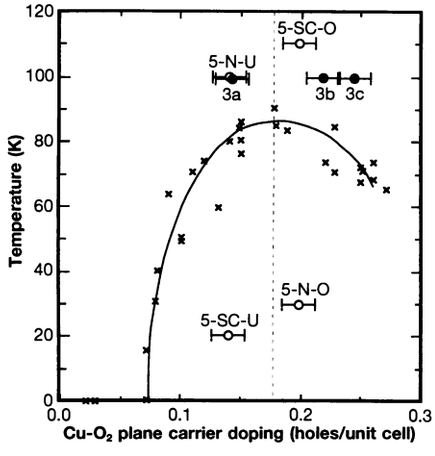

Fig. 1. Location of our measurements in a partial temperature-doping phase diagram. The boundary between the normal and superconducting states is drawn as a line, along with transition data from Groen *et al.* (*14*) (crosses). The circular data points represent some of our experiments at the temperature of the measurement and the doping of the sample; the filled circles mark our first three measurements. The error bars are due to the approximate placement of the transition curve. The points are labeled by the figure number in which their data is presented and the sample name. The dotted line approximately designates optimal doping.

experiments in the phase diagram.

Figure 2 is a 2D **k**-space map, showing part of the LDA Fermi surface for overdoped samples, and the momentum selections for the present data. For the general doping dependence, we use two cuts, or series of spectra, through **k** space. In this Cu-O_2 plane based notation, (0,0) represents zero momentum in the plane, and the (1,0) direction is parallel to the Cu-O bond direction. The coordinates are given in units of (h/a) (where h is Plank's constant, and a is the Cu-O_2 plane lattice constant). The proposed $d_{x^2-y^2}$ superconducting gap has a node along the (0,0)→(π,π) line and a maximum at (π,0).

Throughout this article, we are strictly interested in data from momentum cuts that cross a Fermi surface. For a momentum-integrated experiment, an isotropic gap would be easy to read; it would be the lowest energy with excitations in the spectrum. With ARPES, even in a conventional metal, an arbitrary spectrum is not expected to have weight near E_F. On a cut that crosses a Fermi surface, however, the dispersive feature reaches the lowest binding energy possible before it becomes unoccupied. From the spectra in such a cut, the one with the lowest energy is used to determine the presence of a gap. If there is an excitation gap at that Fermi surface crossing, then there is no longer a Fermi surface; along that surface, however, the feature still loses its weight and reaches a minimum energy. In the case of Bi2212, the Fermi surface terminology is not precise in the first place, because the features are too broad (the excitation lifetimes are too short) for the quasi-particle picture to be accurate (*15*). On the other hand, features in all three samples still lose their spectral weight along a line that is consistent with the LDA Fermi surface, so the quasi-particle–based picture is

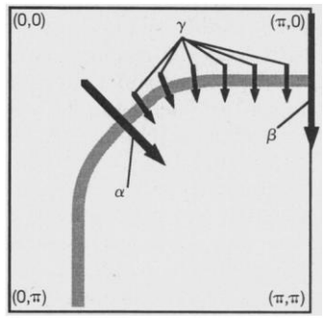

Fig. 2. Map of (one fourth of) the Cu-O_2 plane's first Brillouin zone. The gray line is an experimental Fermi surface from Bi2212 (*33*), corresponding to the bonding Cu-O_2 Fermi surface in LDA calculations (*34*). The four corners are labeled by their two-component momenta, in units of h/a. Black arrows represent momentum cuts on which the data were collected.

not without approximate validity. With the understanding that it may not have the same precise meaning as in more conventional metals, we use the Fermi surface terminology, only to identify the area in momentum space where the dispersive feature loses intensity and the spectral weight reaches its lowest energy. All cuts described here cross an apparent Fermi surface.

Normal state gap. Raw data from the three samples (Fig. 3A) were taken along momentum cuts α and β (Fig. 2). Both cuts cross the LDA Fermi surface, and the α-cut data for all three samples show the Fermi surface crossing behavior expected for a Fermi liquid. As the spectra progress through momentum space, a dispersive feature moves from higher to lower energies until its leading edge is close to E_F. Once there, the feature loses its intensity as the band occupation decreases. Among the β cuts, those from samples b and c are also similar, although the peak dispersion is less pronounced, because of the flat nature of the band in that region. One qualitative change as the doping is reduced (from sample c to a) is that the features become even broader. In the quasi-particle picture, this would imply a decrease in lifetime, as a result of some enhanced scattering. However, this effect also makes the quasi-particle approximation less valid, moving the system further away from such a picture.

We focus mainly on another change in the spectra, the shift of the leading edge in the spectra for the β cuts. The α cuts in Fig. 3A all have similar qualitative characteristics. In each cut, the dispersive features' low-energy edges reach the same level; as they cross the apparent Fermi surface, the lowest excitation energy with weight in the single electron excitation function is the same from sample to sample. The line shape and resolution considerations that determine the exact minimum energy of the spectral weight are relatively constant over the collection of samples, giving us confidence in the similarity of the crossing behaviors. For the β cuts, however, this is not the case: The leading edge of sample a's crossing has receded, or moved to higher energy. On a qualitative level, for some range of the lowest energies with significant spectral weight in samples b and c, there is not significant spectral weight in sample a's spectra along β. Sample c shows the same type of apparent Fermi surface crossing in both cuts, but the same cannot be said for sample a. The missing spectral weight at E_F implies that the spectral weight cutoff for that slice in **k** space is not determined simply by Fermi statistics; there must be an excitation gap.

Because of the lack of a complete theory for the HTS normal state, or even for the ARPES line shape, it is difficult to quantify

this observation, but the different spectra can be compared systematically. One way is to measure the energy of the leading edge's midpoint in each spectrum (Fig. 3B); that is, the energy (lower than the peak's energy) at which the spectral weight is halfway between the peak value and the background (counts with negative binding energy) can be used to characterize the minimum energy excitation within the broad dispersive feature. For five of the Fermi surface crossings, the leading edge energy is minimized at point somewhat closer to (π,π) than the point where the dispersive feature has lost half of its weight. For the remaining cut (β, from sample a), the shape for the midpoint energy, which is always at positive binding energy, is different from that of the other five. Finite instrumental resolution can shift the leading edge toward lower energies, even beyond E_F as determined by the reference sample, but it does so by roughly the same amount for most of the spectra we present. In addition, there is an anomalous, steplike background in all Bi2212 ARPES spectra (*16*), which changes the effective leading-edge midpoint somewhat. This background is roughly isotropic, so one can model it empirically and subtract it from the data. The qualitative features of the cut are unchanged, and the gap effect increases slightly (Fig. 4). Although these caveats should be kept in mind, Fig. 3B still shows that sample a has an excitation gap along the β cut.

It is important to examine closely the criteria for determining the existence of the gap, as the leading edge position has no rigorously defined physical meaning. Comparing the α and β cuts for sample a in Fig. 3B, we can be confident claiming that there is a gap because of the difference in the lowest energy excitations. For this same reason, we know that the gap is anisotropic: it has a different value at different momenta (smaller or zero on the α cut, and larger on the β cut). Situations that would create this effect as an artifact, such as different dispersion rates and varying linewidths, could not produce such a large shift in the leading edge. It is not so easy, however, to determine the absolute magnitude of the gap and whether there is a node along the α cut. We can only estimate the gap size from the leading edge shifts. Comparing the α cut for different samples, the value for sample a is within the scatter of the data points. By studying more samples and getting better statistics, we will be able to set an upper limit on this value. As for the anisotropy of the gap in sample a, the difference in leading edge minima from cut α and β is 20 to 25 meV. This relative measurement is repeated for three more samples, below (*17*).

Gap analysis. The superconducting state also has an excitation gap, and it is important to compare it to the normal state gap. Figure 5 is a comparison of the apparent Fermi surface crossing along cut β for different samples and temperatures. Each spectrum is chosen to have the minimum leading edge energy from a β cut (the feature intensity above the background is not high for either sample, because the leading edge minimum occurs after much of the spectral weight is lost). On a qualitative level, the leading edge is receded from E_F in both the normal and superconducting states of the underdoped sample. For the overdoped sample, the leading edge is close to E_F in the normal state but is pulled back in the superconducting state. Hence, there is an excitation gap in both the normal and superconducting states of the underdoped sample with similar magnitude at the apparent Fermi surface crossing for the β cut.

The most dramatic difference between the underdoped normal and superconducting state spectra is the change in line shape. The superconducting state spectrum has a sharp peak centered at 40 to 50 meV, surrounded by the suppressed spectral weight in the gap region and, at $(\pi,0)$, the higher binding energy dip. Explanations for this feature have been based largely on the presence of an excitation gap (*18*); the resulting lack of phase space for electronic scattering allows a quasi particle with low energy to have a long lifetime. In the normal state spectrum of the underdoped samples, how-

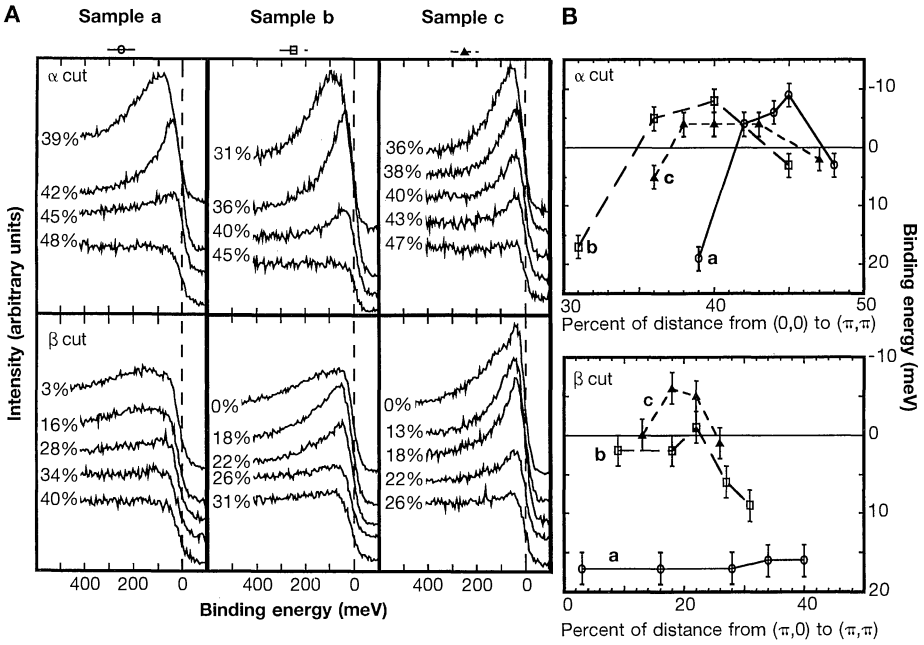

Fig. 3. (**A**) Photoemission spectra from three different samples along momentum cuts α (upper panels) and β (bottom panels), in the normal state (100 K). Sample a was underdoped with T_c = 84 K, and samples b and c were overdoped with T_c = 85 and 80 K, respectively. Each spectrum's momentum is labeled as the percent of the distance from the cut's nominal endpoints. The Fermi energy is indicated by the dotted line. (**B**) Leading-edge midpoint data calculated from the spectra in (A). In each of the cuts (α in the upper panel; β in the lower one), a dispersive feature loses spectral weight. Only in one (sample a on cut β) does the spectral weight fail to reach E_F (solid line).

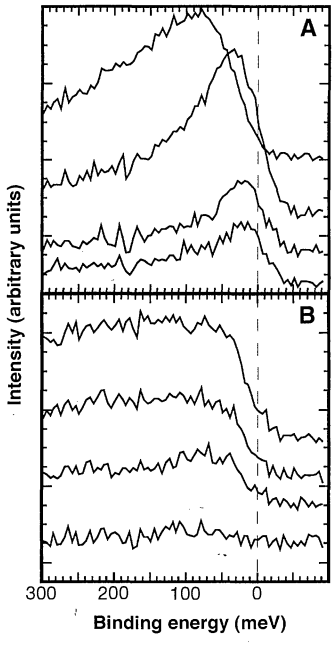

Fig. 4. Background subtraction. The spectra from Fig. 3A, sample a, with the steplike background approximately subtracted. The qualitative behavior is the same as that in Fig. 3. For (**A**) the α cut, the spectral weight reaches E_F (dotted line) as the feature loses intensity. For (**B**) the β cut, the spectral weight does not appreciably reach E_F.

ever, we observe a similar gap, and the sharp feature is not present. In addition, Fig. 6 shows that spectral weight has been transferred from either higher energy or another region in **k** space in the formation of the sharp feature. Any theory which makes a connection between the underdoped normal state gap and the superconducting gap will need to explain this puzzle.

To quantify the anisotropy in the normal state gap according to the methods outlined above, we measured the leading edge midpoints from many cuts (the γ cuts in Fig. 2) taken across the apparent Fermi surface of different underdoped samples (Fig. 7A). The leading edge position remains fairly constant for momenta near the (1,1) direction and then turns to lower energy as one approaches (π,0). This shape is consistent with a wide range of gap functions; the choice depends somewhat on pinning down whether or not the gap is zero along the (1,1) direction. If it is zero, then the so-called "dirty *d*-wave" scenario is likely (*19*). An ansatz gap function for this scenario (maximum of $|d| - c$ and 0, where d is the $d_{x^2-y^2}$ function and c is a constant) has been applied to analysis of optimally doped Bi2212 data (*20*), and for reference, we have drawn a similar line through our data. We cannot determine which leading-edge energy corresponds exactly to zero gap, so the energy position of this line is model dependent. If there is a gap along the (1,1) direction, there are many possible theories, such as a surface effect in which the time-reversal symmetry is broken (*21*).

Figure 7B is a direct comparison of the normal and superconducting state leading edge positions of an underdoped sample, with an overdoped normal state sample for reference. Most importantly, the general shape of the each gap is similar, leading us to suggest that they may have similar origin. The data also show an overall shift, which is partly an artifact of the analysis technique; the sharp feature in the superconducting spectra gives them a significantly different shape. The analysis method may also be partly responsible for the general scatter seen in the data. Surface evolution caused by temperature cycling may also affect the results. Just as in Fig. 7A, however, the scatter of data does not prevent us from unambiguously identifying the existence of an anisotropic gap (contrast with the overdoped data), although it does limit our ability to determine whether the gap along α is zero or not at both temperatures.

One must keep in mind the limitations of this leading edge analysis. It is most reliable for spectra from different momenta in a single sample at the same temperature; we have most confidence in the analysis of the samples shown in Figs. 3 and 7A. The physics is less clear when comparing different samples or different temperatures. Although Fig. 7B shows that the anisotropy of the two gap functions is similar, it is unclear whether the offset between them is truly related to the gap. We cannot rule out the possibility that the offset is evidence for oversimplification in the leading edge analysis, which does not account for effects such as thermal broadening. As for the question of the node along the (1,1) direction, a photoemission measurement can never give a definite answer because of the lack of phase sensitivity. An anisotropic s wave is always a possibility, although for the superconducting state, there is growing evidence for the contrary (*22*).

Theoretical context. The nature of this normal state gap is still unclear. One possibility is an anisotropic spin density wave gap (*23*), which would develop out of antiferromagnetic (AF) ordering in the $Cu\text{-}O_2$ plane as the carrier doping is decreased. In this case, the unit cell doubles in size, together with the number of bands in the Brillouin zone. These

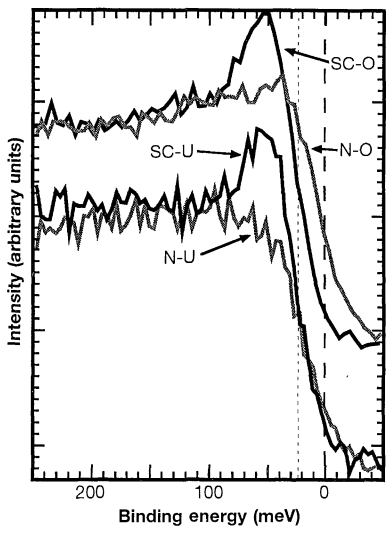

Fig. 5. Normal state (N) and superconducting-state (SC) comparison for underdoped (U) and overdoped (O) samples. The curves correspond to the open dots in Fig. 1 and minimum midpoint energies from cut β; for the underdoped sample, T_c = 83 K, and for the overdoped sample, T_c = 87 K. The heavier dashed line is E_F, which coincides roughly with the leading-edge midpoint of curve N-O. The other midpoints lie near the light dotted line, at a binding energy of roughly 23 meV.

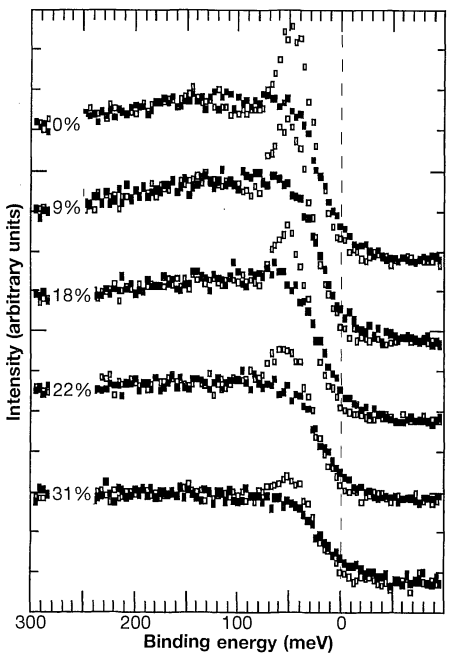

Fig. 6. Comparison of the normal state (solid boxes; 100 K) and superconducting state (open boxes; 20 K) spectra for an underdoped sample (T_c = 83 K) along the β cut. The main difference is the appearance of a sharp feature in the superconducting state, along with slight spectral weight depletion on either side. The feature loses weight around the crossing between (π,0) and (π,π).

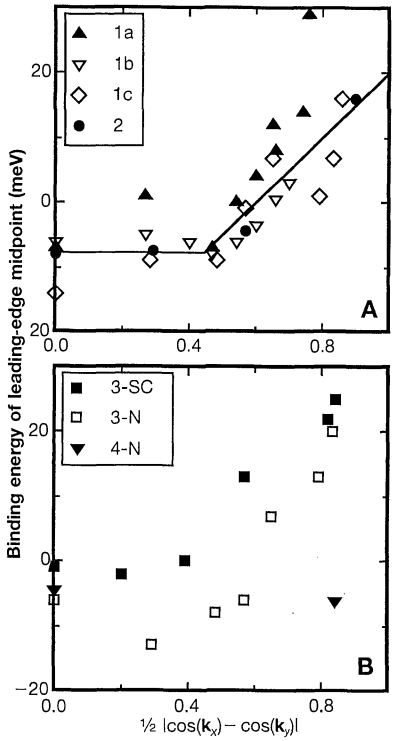

Fig. 7. Leading edge positions from around the LDA Fermi surface for underdoped samples. The values represent the minima from cuts crossing an LDA Fermi surface (γ cuts in Fig. 2). The **k** axis was manipulated to spread the Fermi surface positions out evenly; the $d_{x^2-y^2}$ function is a straight line passing through (0,0) in this graph. (**A**) Two underdoped samples (1 and 2), one of which was examined on three different cleaves (a, b, and c). The solid line is the "dirty *d*-wave" gap function max($|d| - c$, 0), drawn for reference. $T_c(1)$ = 78 K, $T_c(2)$ = 80 K. (**B**) Direct comparison of superconducting state (3-SC) and normal state (3-N) edge positions for an underdoped sample, along with normal state, overdoped data (4-N). $T_c(3)$ = 75 K; $T_c(4)$ = 80 K.

bands interact to form a new band structure with new E_F crossings. This scenario is more likely at even lower hole concentrations, where the AF order is stronger. In the limiting case, results from the insulating parent compound $Sr_2CuO_2Cl_2$ show a structure heavily influenced by AF order (*24*). The dispersive features reach a minimum energy at $(\pi/2,\pi/2)$, and lie at least 200 meV below E_F along the β cut. At very low dopings, features at such an energy would suggest that the low-energy excitations are pockets centered at $(\pm\pi/2,\pm\pi/2)$. Our experiments on further underdoped Bi2212 are, in fact, consistent with this idea (*25*), although further work is required. Recent theoretical efforts have been made to bridge the gap between this picture and the *d*-wave gap scenario, either with a flux state or with a gap magnitude that dramatically increases as the sample's doping decreases (*26*).

Another possible explanation of the normal state gap that is consistent with our observations involves the existence of paired carriers, without long-range coherence (*27, 28*). Essentially, the gap is taken as evidence for a pairing potential in the normal state. Superconductivity, however, does not form without long-range coherence among the pairs, which is established at a lower temperature. Indeed, one can argue from low-temperature London penetration depth measurements (*28*) or from muon spin relaxation experiments (*29*) that the T_c of underdoped samples is determined by the development of phase coherence. The ARPES data will still be sensitive to this gap because they measure the magnitude of the gap and not the phase. This sort of phase diagram has also been proposed in the specific context of novel spin channel $d_{x^2-y^2}$ pairing (*30*), as extensions of the original resonating valence bond idea (*31*). Here, the spin channel pairing strength decreases with increasing carrier concentration, whereas the coherence between pairs increases. In the phase diagram, the two lines (one for pair formation, and one for long-range pair coherence) cross at the doping that achieves maximum T_c, and the superconducting state exists below both lines. This normal state pairing scenario is fundamentally different from the BCS model, in which the coherence between pairs is already sufficient for superconductivity when the pairs are formed. The scenario has also been used to explain many of the deviations from Fermi liquid behavior observed in the normal state of HTS materials (*32*).

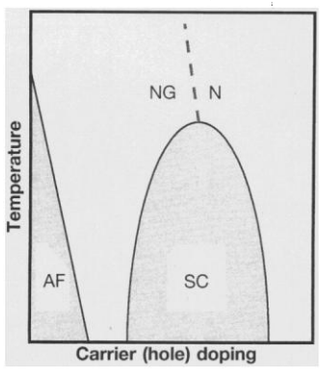

Fig. 8. Sketch of the proposed phase diagram. AF, antiferromagnetic insulator; SC, superconductor; NG, gapped normal state; and N, ungapped normal state. Theories of incoherent pair formation indicate that the dashed line should run diagonally to the upper left, but we do not yet have experimental evidence for this.

The direct observation in our experiment together with data previously reported indicate that we must add to the HTS phase diagram a pseudogapped metallic state (Fig. 8). This excitation gap is anisotropic and roughly the same size as the superconducting gap. The anisotropic nature of this gap may contribute to the scatter in gap sizes reported by other experiments. The boundaries of this state are not known in detail and require further efforts. Closely related areas in need of more data and a better understanding are the evolution (with temperature and doping) of the line shape and the gap magnitude.

REFERENCES AND NOTES

1. For a thorough introduction, see B. Batlogg, *Phys. Today* **44**, 44 (June 1991).
2. J. W. Loram, K. A. Mirza, J. M. Wade, J. R. Cooper, W. Y. Liang, *Physica C* **235**, 134 (1994); J. L. Tallon, J. R. Cooper, P. S. I. P. N. de Silva, G. V. M. Williams, J. W. Loram, *Phys. Rev. Lett.* **75**, 4114 (1995).
3. T. Timusk, private communication. An earlier work done with this technique is L. D. Rotter *et al.*, *Phys. Rev. Lett.* **67**, 2741 (1991).
4. H. Y. Hwang *et al.*, *Phys. Rev. Lett.* **72**, 2636 (1994); B. Batlogg *et al.*, *Physica C* **235**, 130 (1994).
5. M. Takigawa, P. C. Hammel, R. H. Heffner, Z. Fisk, *Phys. Rev. B* **43**, 247 (1991); M. Takigawa, *ibid.* **49**, 4158 (1994); T. Imai *et al.*, *Physica C* **162**, 169 (1989).
6. J. Rossat-Mignod *et al.*, *Physica B* **169**, 58 (1991).
7. Z.-X. Shen *et al.*, *Phys. Rev. Lett.* **70**, 1553 (1993); G. D. Mahan, D. S. Dessau, Z.-X. Shen, D. S. Marshall, *ibid.* **71**, 4277 (1993); (*20*); and references therein.
8. J. Bardeen, L. N. Cooper, J. R. Schrieffer, *Phys. Rev.* **108**, 1175 (1957).
9. For an introduction to the experimental technique, see S. Hüfner, *Photoelectron Spectroscopy* (Springer-Verlag, Berlin, 1995).
10. If the electronic structure is not two-dimensional, the line shape will also have broadening due to the photo-hole lifetime; see N. V. Smith *et al.*, *Phys. Rev. B* **47**, 15476 (1993).
11. The ARPES data presented here were obtained with a Vacuum Science Workshop system, mounted on the undulator beamline 5-3 of the Stanford Synchrotron Radiation Laboratory, at a base pressure of 3×10^{-11} to 5×10^{-11} torr. With 22.4-eV photons, the total energy resolution was typically 25 to 35 meV, and the angular resolution was ±1°. A gold reference sample facilitated energy resolution and Fermi energy measurement to within ±1 meV, and the temperature was known to be accurate to within a few kelvin.
12. The crystals were grown with a directional solidification technique described elsewhere (*13*) and were then annealed to achieve uniform oxygen doping. Carrier reduction resulted from a 600°C anneal in an Argon atmosphere, and higher dopings were achieved with the addition of oxygen to the anneal. We lacked a precise technique for determining the oxygen concentration but characterized carrier concentrations indirectly by measuring T_c with a SQUID magnetometer and comparing the values to the known T_c curve.
13. D. B. Mitzi, L. W. Lombardo, A. Kapitulnik, S. S. Laderman, R. D. Jacowitz, *Phys. Rev. B* **41**, 6564 (1990).
14. W. A. Groen, D. M. de Leeuw, L. F. Feiner, *Physica C* **165**, 55 (1990).
15. D. Pines and P. Nozières, *The Theory of Quantum Liquids* (Benjamin, New York, 1990).
16. All near-E_F ARPES spectra of HTS materials exhibit, to a greater or lesser degree, an unexplained step function. The leading edge is roughly 50 meV broad, with the midpoint at a binding energy of roughly 20 to 25 meV. For a spectrum near pure background, see the 40% spectrum in Fig. 3A for sample a, cut β.
17. One last concern is the possibility that sample a (and similar ones) is bad, in the sense that the spectra are not representative of an underdoped superconductor. In a photoemission experiment, broad, seemingly washed out features are often a sign of a poor sample surface. Whereas the normal-state spectra in Fig. 6 have weak features and lose weight at a receded energy in the manner of sample a in Fig. 3, the superconducting-state spectra show the behavior typical for an overdoped superconductor. The sharp feature, essentially resolution-limited, has a width similar to that in overdoped spectra. One knows that there is not sufficient scattering to affect the momentum resolution (and thus smear out the leading edge) because of the clear momentum dependence of the spectra in Fig. 6. A similar conclusion can be drawn from Fig. 3, sample a, cut α.
18. For an analysis of this line shape, see D. S. Dessau *et al.*, *Phys. Rev. B* **45**, 5095 (1992), and references therein.
19. L. S. Borkowski and P. J. Hirschfeld, *ibid.* **49**, 15404 (1994).
20. M. R. Norman, M. Randeria, H. Ding, J. C. Campuzano, A. F. Bellman, *ibid.* **52**, 15107 (1995).
21. R. B. Laughlin, *Physica C* **234**, 280 (1994).
22. Proceedings of the 1995 Stanford Conference on Spectroscopies in Novel Superconductors, *J. Phys. Chem. Solids* **56** (1995).
23. O. K. Anderson, *ibid.*, p. 1573; J. R. Schrieffer and A. P. Kampf, *ibid.*, p. 1673, and references therein.
24. B. O. Wells *et al.*, *Phys. Rev. Lett.* **74**, 964 (1995).
25. D. S. Marshall, thesis, Stanford University (1996).
26. T. M. Rice, *J. Less-Common Met.* **164** 1439 (1990); X.-G. Wen and P. A. Lee, *Phys. Rev. Lett.* **76**, 503 (1995); L. D. Ioffe and A. J. Millis, in (*22*), p. 1611.
27. S. Doniach and M. Inui, *Phys. Rev. B* **41**, 6668 (1990).
28. V. J. Emery and S. A. Kivelson, *Nature* **374**, 434 (1995).
29. Y. J. Uemura *et al.*, *Phys. Rev. Lett.* **62**, 2317 (1989).
30. T. Tanamoto, K. Kohno, H. Fukuyama, *J. Phys. Soc. Jpn.* **61** 1886 (1992); G. Kotliar and J. Liu, *Phys. Rev. B* **38**, 5142 (1988).
31. P. W. Anderson, *Science* **235**, 1196 (1987).
32. N. Trivedi and M. Randeria, *Phys. Rev. Lett.* **75**, 312 (1995); M. Randeria, N. Trivedi, A. Moreo, R. T. Scalettar, *ibid.* **69**, 2001 (1992).
33. D. S. Marshall *et al.*, unpublished results.
34. S. Massidda, J. Yu, A. J. Freeman, *Physica C* **152**, 251 (1988).

35. We gratefully acknowledge discussions with S. Kivelson, R. B. Laughlin, P. A. Lee, X.-G. Wen, S. Doniach, H. Fukuyama, N. Nagaosa, A. J. Millis, D. J. Scalapino, and N. Bulut. The data presented here were obtained from the Stanford Synchrotron Radiation Laboratory (SSRL), which is operated by the U.S. Department of Energy (DOE) Office of Basic Energy Sciences, Division of Chemical Sciences. The Office's Division of Materials Science has provided support for this research. The Stanford work was also supported by NSF grants DMR-9311566 and DMR-9357507. Beamline 5 of SSRL was built with DARPA, ONR, AFOSR, AOR, DOE, and NSF support.

4 March 1996; accepted 24 May 1996